

Supplementary Material for

**Older than they look:
cryptic recycled xenotime on detrital zircon**

Maximilian Dröllner¹, Milo Barham¹, Christopher L. Kirkland¹, and Malcolm P. Roberts²

¹Timescales of Mineral Systems Group, The Institute of Geoscience Research, School of Earth and Planetary Sciences, Curtin University, GPO Box U1987, Perth, WA 6845, Australia

²Centre for Microscopy, Characterisation and Analysis (CMCA), The University of Western Australia, Perth, WA 6009, Australia

Supplemental Material S1: Detailed analytical methods (provided below)

Supplemental Material S2: Data tables S1–S7 (Excel workbook)

SUPPLEMENTARY MATERIAL S1

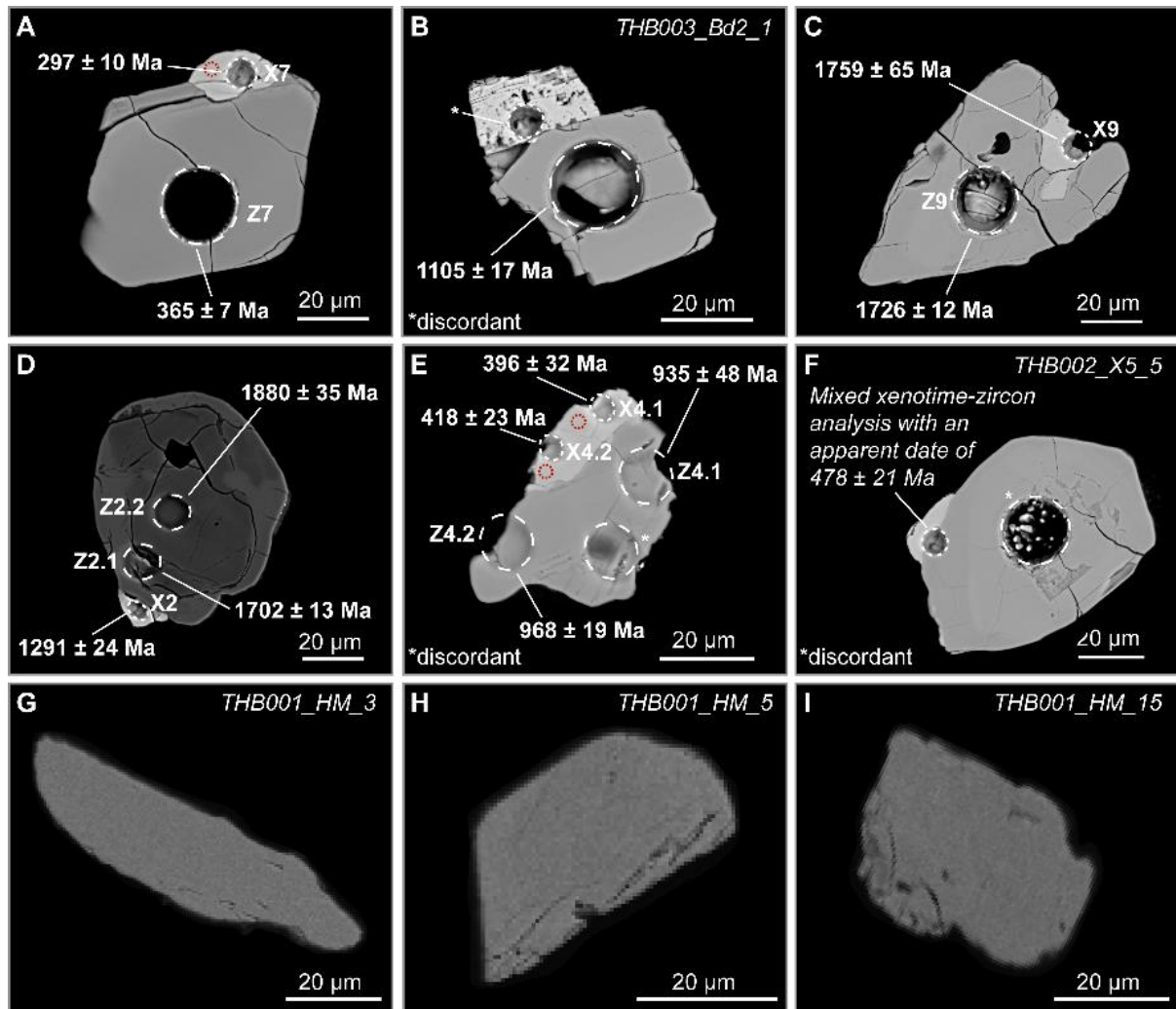


Figure S1: Additional examples of backscattered electron images (no standardized brightness/contrast) of grains analyzed in this study. Coding (e.g., X7) is from Table S2-S7 in the Supplementary Material S2 (consistent with Fig. 3), where X = xenotime and Z = zircon. Images without coding are not shown in the paper (e.g., because they represent analytical mixtures of xenotime and zircon) and show the associated Analysis ID in the upper right corner (compare with supplementary tables). (A-C, F) Xenotime outgrowths and zircon grains dated using LA-ICP-MS. (B) Discordant xenotime outgrowth; note inclusion-rich texture possibly suggesting different formation environment. (C) Apparent xenotime inclusion with an age that is indistinguishable from its zircon host. (D-E) Xenotime outgrowths and zircon grains dated using SIMS. (F) Mixed xenotime-zircon analysis providing meaningless date. Most mixed analysis plot near the group of youngest xenotime outgrowths (Fig. 3A,B), which is consistent with mixed analysis representing similarly old xenotime outgrowths mixed with older zircon substrates, and hence supporting the conclusions of this work. (G-I) Detrital xenotime grains (pre-analysis).

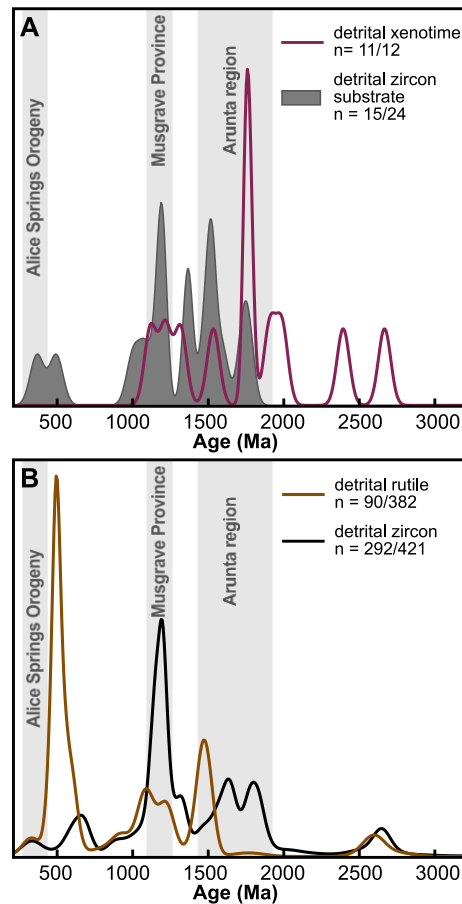


Figure S2: Kernel density estimates (KDE) of Broome Sandstone detritus. (A) U-Pb ages of detrital zircon substrate bearing xenotime, detrital xenotime, (B) detrital zircon, and detrital rutile (both Dröllner et al., 2023).

METHODS

Sample preparation and phase identification

The presented work studied four samples, three (THB001, THB002, THB003) are derived from the poorly consolidated to unconsolidated Thunderbird heavy mineral sand deposit that is attributed to the Broome Sandstone (Boyd and Teakle, 2016). The other sample (GPT001) is a moderately well consolidated sandstone collected from the outcropping Broome Sandstone (location provided in Table S1 within Supplementary Material S2). Sample GPT001 was subjected to high voltage electrical fragmentation (Selfrag Lab, Switzerland) to liberate the minerals. The subsequent steps of mineral separation were the same for all disaggregated sediment samples and involved the use of a Jasper Canyon Research zircon shaking table (as described in Dumitru, 2016), heavy liquid separation (using a density of 2.85 g/cm³), and magnetic separation using a Frantz isodynamic magnetic separator. Representative splits of the zircon-rich heavy mineral separates were bulk-mounted, i.e., representative sample splits of grains were mounted by affixing them on double-sided tape and embedding them in epoxy resin. The mounts were then polished to expose the grain interiors. Automated mineral identification and mapping were performed using energy-dispersive X-ray

spectrometry (EDX) and backscattered electron imaging on the TESCAN Integrated Mineral Analyzer (TIMA, Czech Republic). The TIMA instrument, a field emission scanning electron microscope equipped with energy-dispersive spectroscopy detectors, was used to perform automated phase identification of minerals. The measurements were taken using TIMA's liberation analysis with dot mapping (using BSE and EDS with step sizes of 1 and 3 μm), a beam energy of 25 kV, a probe current of 5.4 nA, and a spot size of 79.2 nm. In brief, the TIMA compares EDX spectra of unknowns with a database of EDX spectra built from known mineral reference materials; a demonstration of TIMA's functionality is provided by Hrstka et al. (2018). Automated phase identification for a single 25 mm round mount took *c.* 3 hrs. A typical mount hosted over 10,000 identified zircon grains. Of these grains, between 0.1 and 1% showed resolvable xenotime outgrowths, and typically only a few were sufficiently large to allow spot analysis. Mineralogical maps from the TIMA were used to guide geochronological analyses.

Xenotime U-Pb geochronology

Xenotime minerals were analyzed by laser ablation-inductively coupled plasma-mass spectrometry (LA-ICP-MS) and secondary ion mass spectrometry (SIMS) at Curtin University's John de Laeter Centre (Perth, Australia). All ages are single analysis Concordia ages (unless otherwise stated) and uncertainties are 2σ . The use of Concordia ages (Ludwig, 1998) avoids changing between different ratios ($^{207}\text{Pb}/^{206}\text{Pb}$ and $^{206}\text{Pb}/^{238}\text{U}$) for age calculation, (ii) optimizes varying uncertainty within both U/Pb and Pb/Pb ratios through time (Ludwig, 1998; Zimmermann et al., 2018), and (iii) provides a less biased approach to discordance (Vermeesch, 2021).

LA-ICP-MS

Measurements used a RESolution 193 nm excimer laser with a laser fluence of 2.1 J cm^{-2} and repetition rate of 5 Hz for *c.* 30 s analysis time. Background capture time was 30 s. The sample cell was flushed by ultrahigh purity He (0.32 L min^{-1}) and N_2 (1.2 mL min^{-1}). Circular spot sizes of *c.* 7 μm (pit depths of *c.* 3 μm and *c.* 70 μm^3 analytical volume; measured using a ZetaTM-20 Optical Profiler) and 10 μm were used for xenotime outgrowths and detrital xenotime grains (and their associated reference materials), respectively. U-Pb analysis employed an Agilent 8900 Triple Quadrupole ICP-MS monitoring for ^{91}Zr , ^{202}Hg , ^{204}Pb , ^{206}Pb , ^{207}Pb , ^{208}Pb (0.1 s dwell time on all Pb isotopes), ^{232}Th (0.025 s dwell time), and ^{238}U (0.025 s dwell time). The primary xenotime reference material was the z6413 xenotime ($^{206}\text{Pb}/^{238}\text{U}$ age = 994 ± 1 , $^{207}\text{Pb}/^{206}\text{Pb}$ age = 997 ± 1 Ma; Stern and Rayner, 2003), while the MG-1 xenotime ($^{206}\text{Pb}/^{238}\text{U}$ age = 490 ± 1 Ma; $^{207}\text{Pb}/^{206}\text{Pb}$ age = 492 ± 1 Ma; Fletcher et al., 2004) was used as a secondary reference material and has been analyzed at regular intervals to scrutinize precision and accuracy. The time-resolved mass spectra were reduced using the U-Pb Geochronology data reduction scheme in Iolite 4 (Paton et al., 2011 and references therein). Subsequent to the analysis, ablation spots were controlled for any evidence for mixing xenotime and

zircon (e.g., Fig. S1F). Additionally, ^{91}Zr has been monitored during data reduction and used as a semi-quantitative measure of contamination by zircon. Analyses that have been classified based on visual inspection as “Potential zircon component to analysis” and “Mixed xenotime-zircon analysis” (Table S4) commonly showed increased levels of ^{91}Zr , compared to analyses classified as “Pure xenotime analysis” that show low levels of ^{91}Zr consistent with Zr contents measured using EPMA (Table S7). ^{204}Pb was monitored but did not exceed detection limits for near-concordant analyses and data have not been corrected for common Pb. Ages were calculated using the IsoplotR software (Vermeesch, 2018). Results of the secondary reference material for 7 μm spot sizes ($^{206}\text{Pb}/^{238}\text{U}$ age = 492 ± 9 Ma, MSWD = 2.14; $^{207}\text{Pb}/^{206}\text{Pb}$ age = 529 ± 143 Ma, MSWD = 3.0; $n = 5/5$) and for 10 μm ($^{206}\text{Pb}/^{238}\text{U}$ age = 491 ± 8 Ma, MSWD = 0.37; $^{207}\text{Pb}/^{206}\text{Pb}$ age = 530 ± 117 Ma, MSWD = 0.8; $n = 5/5$) are indistinguishable from published values. If multiple spots of individual detrital xenotime grains were measured, the weighted means of the measured isotope ratios were used for Concordia and kernel density estimates.

SIMS

Measurements used a SHRIMP II instrument and a spot size of $c. 8 \times 7 \mu\text{m}$ (pit depths of $c. 1 \mu\text{m}$ and $c. 15 \mu\text{m}^3$ analytical volume); measured using a ZetaTM-20 Optical Profiler). Analysis sites were cleaned before analysis by rastering the primary ion beam over the target area for two minutes. Unknowns and reference materials were mounted on different mounts. Prior to analysis, both mounts were cleaned and gold coated together. Three in-house xenotime reference materials of different age and composition (provided by Allen Kennedy, Curtin University) were used (Cavosie et al., 2021). Measurements used a beam current of ~ 0.2 nA and seven scans of the mass spectrum were recorded for individual analysis monitoring $^{194}\text{Y}_2\text{O}^+$, $^{196}\text{Zr}_2\text{O}^+$, $^{204}\text{Pb}^+$, background ($^{204}\text{Pb}^+ + 0.00946$ AMU offset), $^{206}\text{Pb}^+$, $^{207}\text{Pb}^+$, $^{208}\text{Pb}^+$, $^{248}\text{ThO}^+$, $^{254}\text{UO}^+$, $^{264}\text{ThO}_2^+$, and $^{270}\text{UO}_2^+$. U-Pb isotopic ratios and absolute abundances were determined relative to a ca. 950 Ma xenotime reference material with ca. 20000 ppm U and ca. 10000 ppm Th. SQUID III software (Bodorkos et al., 2020) was used for data reduction and ages were calculated using the IsoplotR software (Vermeesch, 2018). Calibrations were performed using a regression through $\ln(^{206}\text{Pb}^+/^{254}\text{UO}^+)$ versus $\ln(^{270}\text{UO}^+/^{254}\text{UO}^+)$. U-Pb SIMS data were corrected for common lead using the measured ^{204}Pb and the two-stage terrestrial Pb evolution model of Stacey and Kramers (1975). Ages were corrected for matrix differences between primary reference material and unknowns using the method of Fletcher et al. (2004). Uncertainties of U, Th, and ΣREE are propagated in quadrature to the external $^{206}\text{Pb}/^{238}\text{U}$ uncertainty. Ages of two in-house secondary reference materials are in good agreement with the expected TIMS U-Pb values (Table S2). These two reference materials differ significantly in their age and composition: One has a Paleozoic age and low U and Th concentration, the other has an Archean age and high U and Th concentrations. It is notable that SIMS U-Pb geochronology is susceptible to matrix effects that can affect the robustness of the U/Pb ages (Fletcher et al., 2004; Cross and Williams, 2018). Although this may suggest the use

of $^{207}\text{Pb}/^{206}\text{Pb}$ ages are preferred over $^{206}\text{Pb}/^{238}\text{U}$ ages, it is important to consider that the specific xenotime analyses herein (i.e., outgrowths) are apparently young (i.e., Paleozoic). Therefore, limited radiogenic ingrowth of ^{207}Pb hampers the precision of the $^{207}\text{Pb}/^{206}\text{Pb}$ geochronometer. Limited robustness of $^{207}\text{Pb}/^{206}\text{Pb}$ ages and the good reproducibility of $^{206}\text{Pb}/^{238}\text{U}$ ages (after matrix effect correction) of secondary xenotime reference materials, suggest that the full suite of U and Pb isotopic data can be used to derive an age of xenotime formation (e.g., by using single analysis Concordia ages).

Zircon U-Pb geochronology

Zircon minerals were analyzed by laser ablation-inductively coupled plasma-mass spectrometry (LA-ICP-MS) and secondary ion mass spectrometer (SIMS) at Curtin University's John de Laeter Centre (Perth, Australia). All ages are single analysis Concordia ages (unless otherwise stated) and uncertainties are 2σ . The use of Concordia ages (Ludwig, 1998) avoids changing between different ratios ($^{207}\text{Pb}/^{206}\text{Pb}$ and $^{206}\text{Pb}/^{238}\text{U}$) for age calculation, (ii) optimizes varying uncertainty within both U/Pb and Pb/Pb ratios through time (Ludwig, 1998; Zimmermann et al., 2018), and (iii) provides a less biased approach to discordance (Vermeesch, 2021).

LA-ICP-MS

Measurements used a RESolution 193 nm excimer laser with a laser fluence of 2.4 J cm^{-2} and repetition rate of 5 Hz for *c.* 30 s analysis time. Background capture time was 30 s. The sample cell was flushed by ultrahigh purity He (0.68 L min^{-1}) and N_2 (2.8 mL min^{-1}). A circular spot size of 20 μm was used. U-Pb analysis employed an Agilent 8900 Triple Quadrupole ICP-MS monitoring for ^{202}Hg , ^{204}Pb , ^{206}Pb , ^{207}Pb , ^{208}Pb (0.1 s dwell time on all Pb isotopes), ^{232}Th (0.025 s dwell time), and ^{238}U (0.025 s dwell time). The primary reference material was the GJ1 zircon ($^{206}\text{Pb}/^{238}\text{U}$ age = 602 ± 1 , $^{207}\text{Pb}/^{206}\text{Pb}$ age = 602 ± 1 Ma; Jackson et al., 2004), while the 91500 zircon ($^{206}\text{Pb}/^{238}\text{U}$ age = 1065 ± 1 Ma; $^{207}\text{Pb}/^{206}\text{Pb}$ age = 1065 ± 1 Ma; Wiedenbeck et al., 1995) and the OGC/OG-1 zircon ($^{207}\text{Pb}/^{206}\text{Pb}$ age = 3465 ± 1 Ma; Stern et al., 2009) were used as secondary reference materials and have been analyzed at regular intervals to scrutinize precision and accuracy. Time-resolved mass spectra were reduced using the U–Pb Geochronology data reduction scheme in Iolite 4 (Paton et al., 2011 and references therein). ^{204}Pb has been monitored but did not exceed detection limits for near-concordant analyses and data have not been corrected for common Pb. Errors were propagated using the method integrated in Iolite4 (Paton et al., 2011). Ages were calculated using the IsoplotR software (Vermeesch, 2018). Weighted mean ages of secondary reference materials 91500 ($^{206}\text{Pb}/^{238}\text{U}$ age = 1060 ± 6 Ma, MSWD = 0.3; $n=11/11$) and OGC ($^{207}\text{Pb}/^{206}\text{Pb}$ age = 3461 ± 89 Ma, MSWD = 0.2; $n=11/11$) are indistinguishable with published values.

SIMS

Measurements used a SHRIMP II with a spot size of $c. 14 \times 12 \mu\text{m}$. Analysis sites were cleaned before analysis by rastering the primary ion beam over the target area for two minutes. U-Pb isotopic ratios were quantified relative to the BR266/z6266 reference zircon with an $^{206}\text{Pb}/^{238}\text{U}$ age = 559.0 ± 0.2 Ma and an $^{207}\text{Pb}/^{206}\text{Pb}$ age = 562.6 ± 0.2 Ma (Stern and Amelin, 2003). Analysis of primary reference material were interspersed with analyses of the OGC/OG-1 zircon ($^{207}\text{Pb}/^{206}\text{Pb}$ age = 3465 ± 1 Ma; Stern et al., 2009) to monitor accuracy and precision. SQUID III software (Bodorkos et al., 2020) was used for data reduction and ages were calculated using the IsoplotR software (Vermeesch, 2018). U-Pb SIMS data were corrected for common lead using the measured ^{204}Pb and the two-stage terrestrial Pb evolution model of Stacey and Kramers (1975). OGC yielded a ^{204}Pb -corrected weighted mean $^{207}\text{Pb}/^{206}\text{Pb}$ age of 3469 ± 19 Ma (MSWD = 0.8; $n = 4$) consistent with the reported age. Provided uncertainties of zircon ages are external measurement errors.

Electron probe micro-analyzer

Quantitative elemental analyses were acquired on a JEOL JXA8530F Hyperprobe at the CMCA, Western Australia. Operating conditions were 40 degrees take-off angle, and a beam energy of 25 keV. This instrument is equipped with 5 tunable wavelength dispersive spectrometers. The beam current was 50 nA for calibration and 100 nA for unknown sample measurement. The electron beam diameter was defocussed to 3 microns to reduce the effects of beam drift and sample damage during analysis. The instrument was initially calibrated, and the unknowns acquired using the Probe for EPMA[®] software package (Probe Software[®]).

Standards used for instrument calibration were a selection of in-house silicates and Drake and Weill glasses and USNM REE phosphates from the Smithsonian Institute.

The elements were acquired using analysing crystals LiFH for Ho $\text{I}\beta$, Yb $\text{I}\alpha$, Lu $\text{I}\beta$, Eu $\text{I}\alpha$, Tb $\text{I}\alpha$, Tm $\text{I}\alpha$, LiF for Er $\text{I}\alpha$, Nd $\text{I}\alpha$, Sm $\text{I}\alpha$, Gd $\text{I}\alpha$, Dy $\text{I}\alpha$, PETJ for U $\text{m}\beta$, Zr $\text{I}\alpha$, Y $\text{I}\alpha$, P $\text{K}\alpha$, Ca $\text{K}\alpha$, Th $\text{m}\alpha$, and TAP for Si $\text{K}\alpha$. The on-peak count times were 20 seconds for Y $\text{I}\alpha$, P $\text{K}\alpha$, Ca $\text{K}\alpha$, Lu $\text{I}\beta$, Eu $\text{I}\alpha$, Tb $\text{I}\alpha$, Tm $\text{I}\alpha$, Nd $\text{I}\alpha$, Sm $\text{I}\alpha$, Gd $\text{I}\alpha$, 30 seconds for Er $\text{I}\alpha$, Yb $\text{I}\alpha$, Ho $\text{I}\beta$, Dy $\text{I}\alpha$, 60 seconds for U $\text{m}\beta$, Th $\text{m}\alpha$, 80 seconds for Zr $\text{I}\alpha$, and 150 seconds for Si $\text{K}\alpha$. Off peak counting time were 20 seconds for Y $\text{I}\alpha$, P $\text{K}\alpha$, Ca $\text{K}\alpha$, Lu $\text{I}\beta$, Eu $\text{I}\alpha$, Tb $\text{I}\alpha$, Tm $\text{I}\alpha$, Nd $\text{I}\alpha$, Sm $\text{I}\alpha$, Gd $\text{I}\alpha$, 30 seconds for Er $\text{I}\alpha$, Yb $\text{I}\alpha$, Ho $\text{I}\beta$, Dy $\text{I}\alpha$, 60 seconds for U $\text{m}\beta$, Th $\text{m}\alpha$, 80 seconds for Zr $\text{I}\alpha$, and 150 seconds for Si $\text{K}\alpha$. Off Peak correction method was Linear for Zr $\text{I}\alpha$, Si $\text{K}\alpha$, Y $\text{I}\alpha$, P $\text{K}\alpha$, Th $\text{m}\alpha$, Ho $\text{I}\beta$, Er $\text{I}\alpha$, Yb $\text{I}\alpha$, Lu $\text{I}\beta$, Eu $\text{I}\alpha$, Nd $\text{I}\alpha$, Sm $\text{I}\alpha$, Gd $\text{I}\alpha$, Dy $\text{I}\alpha$, Exponential for U $\text{m}\beta$, Ca $\text{K}\alpha$, and Slope (Hi) for Tb $\text{I}\alpha$, Tm $\text{I}\alpha$.

Unknown and standard intensities were corrected for deadtime. Standard intensities were corrected for standard drift over time. Oxygen was calculated by cation stoichiometry and included in the matrix

correction (Donovan et al., 1992). The Phi-Rho-Z algorithm utilized was Armstrong/Love Scott (Armstrong, 1988).

Shape coefficients were calculated using the BLambdaR software (Anenburg and Williams, 2022).

References cited

- Anenburg, M., and Williams, M.J., 2022, Quantifying the Tetrad Effect, Shape Components, and Ce–Eu–Gd Anomalies in Rare Earth Element Patterns: *Mathematical Geosciences*, v. 54, no. 1, p. 47–70, doi: 10.1007/s11004-021-09959-5.
- Armstrong, J.T., 1988, Quantitative analysis of silicate and oxide materials: comparison of Monte Carlo, ZAF, and ψ (pZ) procedures: *Microbeam analysis*, p. 239–246.
- Bodorkos, S., Bowring, J.F., and Rayner, N.M., 2020, Squid3: next-generation data processing software for sensitive high-resolution ion microprobe (SHRIMP).
- Boyd, D.M., and Teakle, M.G., 2016, Thunderbird heavy mineral sand deposit, Western Australia: *Applied Earth Science*, v. 125, no. 3, p. 128–139, doi: 10.1080/03717453.2016.1200268.
- Cavosie, A.J., Kirkland, C.L., Reddy, S.M., Timms, N.E., Talavera, C., and Pincus, M.R., 2021, Extreme plastic deformation and subsequent Pb loss in shocked xenotime from the Vredefort Dome, South Africa, *in* Reimold, W.U., Koeberl, C., eds., *Large Meteorite Impacts and Planetary Evolution VI*, Geological Society of America, p. 465–478.
- Cross, A.J., and Williams, I.S., 2018, SHRIMP U–Pb–Th xenotime (YPO₄) geochronology: A novel approach for the correction of SIMS matrix effects: *Chemical Geology*, v. 484, p. 81–108, doi: 10.1016/j.chemgeo.2017.12.017.
- Donovan, J.J., Snyder, D.A., and Rivers, M.L., 1992, An improved interference correction for trace element analysis, *in* *Proceedings of the Annual Meeting-Electron Microscopy Society of America*, San Francisco Press.
- Dröllner, M., Barham, M., and Kirkland, C.L., 2023, Reorganization of continent-scale sediment routing based on detrital zircon and rutile multi-proxy analysis: *Basin Research*, v. 35, no. 1, p. 363–386, doi: 10.1111/bre.12715.
- Dumitru, T.A., 2016, A new zircon concentrating table designed for geochronologists: *AGU Fall Meeting Abstracts*.
- Fletcher, I.R., McNaughton, N.J., Aleinikoff, J.A., Rasmussen, B., and Kamo, S.L., 2004, Improved calibration procedures and new standards for U–Pb and Th–Pb dating of Phanerozoic xenotime by ion microprobe: *Chemical Geology*, v. 209, 3-4, p. 295–314, doi: 10.1016/j.chemgeo.2004.06.015.
- Hrstka, T., Gottlieb, P., Skála, R., Breiter, K., and Motl, D., 2018, Automated mineralogy and petrology - applications of TESCAN Integrated Mineral Analyzer (TIMA): *Journal of Geosciences*, v. 63, p. 47–63, doi: 10.3190/jgeosci.250.
- Jackson, S.E., Pearson, N.J., Griffin, W.L., and Belousova, E.A., 2004, The application of laser ablation-inductively coupled plasma-mass spectrometry to in situ U–Pb zircon geochronology: *Chemical Geology*, v. 211, 1-2, p. 47–69, doi: 10.1016/j.chemgeo.2004.06.017.

- Ludwig, K.R., 1998, On the Treatment of Concordant Uranium-Lead Ages: *Geochimica et Cosmochimica Acta*, v. 62, no. 4, p. 665–676, doi: 10.1016/S0016-7037(98)00059-3.
- Paton, C., Hellstrom, J., Paul, B., Woodhead, J., and Hergt, J., 2011, Iolite: Freeware for the visualisation and processing of mass spectrometric data: *Journal of Analytical Atomic Spectrometry*, v. 26, no. 12, p. 2508, doi: 10.1039/c1ja10172b.
- Stacey, J.S., and Kramers, J.D., 1975, Approximation of terrestrial lead isotope evolution by a two-stage model: *Earth and Planetary Science Letters*, v. 26, no. 2, p. 207–221, doi: 10.1016/0012-821X(75)90088-6.
- Stern, R.A., and Amelin, Y., 2003, Assessment of errors in SIMS zircon U–Pb geochronology using a natural zircon standard and NIST SRM 610 glass: *Chemical Geology*, v. 197, 1–4, p. 111–142, doi: 10.1016/S0009-2541(02)00320-0.
- Stern, R.A., Bodorkos, S., Kamo, S.L., Hickman, A.H., and Corfu, F., 2009, Measurement of SIMS Instrumental Mass Fractionation of Pb Isotopes During Zircon Dating: *Geostandards and Geoanalytical Research*, v. 33, no. 2, p. 145–168, doi: 10.1111/j.1751-908X.2009.00023.x.
- Stern, R.A., and Rayner, N., 2003, Ages of several xenotime megacrysts by ID-TIMS: potential reference materials for ion microprobe U–Pb geochronology, 9 p.
- Vermeesch, P., 2018, IsoplotR: A free and open toolbox for geochronology: *Geoscience Frontiers*, v. 9, no. 5, p. 1479–1493, doi: 10.1016/j.gsf.2018.04.001.
- Vermeesch, P., 2021, On the treatment of discordant detrital zircon U–Pb data: *Geochronology*, v. 3, no. 1, p. 247–257, doi: 10.5194/gchron-3-247-2021.
- Wiedenbeck, M., Allé, P., Corfu, F., Griffin, W.L., Meier, M., Oberli, F., and Quadt, A. von, 1995, Three Natural Zircon Standards for U–Th–Pb, Lu–Hf, Trace Element and REE Analyses: *Geostandards and Geoanalytical Research*, v. 19, no. 1, p. 1–23, doi: 10.1111/j.1751-908X.1995.tb00147.x.
- Zimmermann, S., Mark, C., Chew, D., and Voice, P.J., 2018, Maximising data and precision from detrital zircon U–Pb analysis by LA-ICPMS: The use of core-rim ages and the single-analysis concordia age: *Sedimentary Geology*, v. 375, p. 5–13, doi: 10.1016/j.sedgeo.2017.12.020.